Hindawi
International Transactions on Electrical Energy Systems
Volume 2022, Article ID 9161590, 18 pages
https://doi.org/10.1155/2022/9161590

Research Article

Suppression to Angular Oscillation among Synchronous Generators by Optimizing Parameters and Set-Points of Synchronous Condenser and High-Voltage DC

Shenghu Li,[1,2] **Diwen Tao**,[1,2] **Lulu Li**,[1,2] **Nan Qi**,[1,2] **and Junwei Gong**[1,2]

[1]*School of Electrical Engineering and Automation, Hefei University of Technology, Hefei 230009, China*
[2]*Anhui Province Key Laboratory of Renewable Energy Utilization and Energy Saving, Hefei 230009, China*

Correspondence should be addressed to Shenghu Li; shenghuli@hfut.edu.cn

Received 25 October 2022; Revised 24 November 2022; Accepted 10 December 2022; Published 22 December 2022

Academic Editor: Mahdiyeh Eslami

After losing one or two poles of the high-voltage DC (HVDC) line, power systems may experience angular oscillations among the synchronous generators (SGs), possibly followed by tripping of the SGs and blackouts of the loads. To suppress the oscillations, the difficulty lies in the optimization methods and the countermeasures. For the former, parameter optimization based on the eigen-analysis for a given scenario is not suitable for angular oscillation after a large disturbance lasting for several seconds or longer. For the latter, adjusting the active power of the SGs is effective but responds slowly. Adjusting the excitation system of the synchronous condensers (SCs) is seldom studied since the relation of the power angle with the reactive power is not clearly described. Adjusting the control parameters of the remaining HVDC has limited effect and is not enough. The set-points for the controller of the HVDC are adjusted to suppress the oscillation but are to be restored after the oscillation, which is different from optimization of the control parameters. In this paper, coordinated optimization of the control parameters and the set-points of the SC and the HVDC is proposed to suppress the angular oscillations among the SGs. At first, the relation of the reactive power of the SC with the power angles is validated to provide the basis for optimizing the control parameters and the set-points of the SC. Since the analytical expression between the power angle and the control parameters or the set-points related to the reactive power is not explicit and the optimization periods of different parameters are different, an improved analytical model of the trajectory sensitivity (TS) is proposed. Based on the indication indices, the control parameters and the set-points of the constant current controller and the excitation system to be optimized are decided. The gradients of the objective function are extended to derive a coordinated multiparameter optimization model to suppress the angular oscillation among the SGs. The numerical results validate the accuracy of the improved TS by comparing it with the perturbation method. The time-domain analysis in different scenarios shows that the angular oscillations in the AC/HVDC system are effectively suppressed with the proposed optimization model.

1. Introduction

The angular oscillation among the synchronous generators (SGs) after large disturbances endangers the security of the power systems. To suppress the oscillations, one may introduce the supplementary controllers, e.g., the power system stabilizer (PSS) of the SGs or the power oscillation damper of the doubly-fed induction generators (DFIGs) [1, 2], or adjust the output of the DFIGs or the energy storage [3, 4]. In [5], the parameters of the PSS and the static var compensator are optimized in coordination with the particle swarm optimization (PSO) to suppress the oscillations. In [6], the tuning scheme of the PSS is proposed to suppress local and interarea mode oscillations with the weight function of the angular velocity deviation and the damping time. With the high-voltage DC (HVDC) widely applied [7], the oscillation in the AC/HVDC power system is more complex and needs to be suppressed [8, 9]. One may adjust the output of the SGs or the doubly-fed induction generators (DFIGs), curtail the loads, introduce the supplementary control, or optimize the parameters of the controllers. The latter is more economical and may be applied to the HVDC

[10, 11] and the AC equipment [12, 13]. The energy storage system is applied to suppress the oscillation based on the model predictive control [14]. The impact of the control parameters of the DFIG on the oscillation is verified by the eigen-analysis [15, 16].

As seen in [17], increasing the reactive power of the synchronous generator (SC) may suppress the oscillation, but the existing studies focus on optimization to the active power and ignore the effect of the reactive power on the oscillation. In [18], the improved active/reactive power control of DFIG is proposed to damp the interarea low-frequency oscillation. In [19], the optimization model of the DC power and the capacitors is proposed by simplifying the nonlinear control model into the quadratic programming model. The suppression schemes are independent, without coordinating the HVDC and other equipment. Tuning parameters is often for the control parameters, while little attention is given to the set-points. In [20], power system stability is investigated by adjusting the set-points of the HVDC in the small-signal stability analysis. The set-points are optimized to enhance the dynamic response during and after the fault with automatic adjustment [21, 22].

To suppress the angular oscillation in the AC/HVDC power system, some difficulties are to be solved.

(1) How to coordinate the parameters of both the HVDC and the AC equipment. The manual adjustment is not practical for multiple parameters, hence coordinated optimization is required. But many optimization models use the heuristic methods, which are easy to implement but are time-consuming and may not achieve global optimization. An analytical optimization model is needed.

(2) How to quantify the relation between the power angles of the SGs and the parameters and decide which parameters should be optimized. The eigen-sensitivity model [23, 24] based on the linearized system model at a given operating point is not suitable for large disturbances, followed by a dynamic process lasting for several seconds. The trajectory sensitivity (TS) quantifies the relationship between the dynamic response and faults or large disturbances [25, 26]. In [27], the optimization to the PSS is proposed with the trajectory sensitivity and the conjugate gradient method. In [28], the control parameters of the DFIG are optimized with the PSO and the trajectory sensitivity. It may be derived by the perturbation method or the analytical method [29, 30]. The former is simpler but requires more calculations. The latter is computationally more efficient for adjusting multiple parameters. It is difficult to derive the analytical expression of the TS from the parameters related to the active and reactive powers since the latter may be shown in the power flow equations instead of the dynamic modeling [31].

(3) How to optimization to the control parameters and the set-points together. The control parameters, such as PI parameters and time constants, affect the dynamic process but have no impact during the steady state. They are often adjusted before the transient process. The set-points of the voltage or current will change both power flow and the postfault dynamic response [32]. For example, temporarily changing the reference of the constant current control (CCC) of the nonfault pole helps to suppress oscillation [33]. Adjusting the set-points of voltage and power helps to delay the critical clearing time and maintain system stability [34]. However, it is difficult to derive the TS-based optimization model for the control parameters and the set-points, because they have different periods of optimization.

To suppress the angular oscillation among the SGs, this paper proposes a coordinated optimization model for the HVDC and the SC based on the trajectory sensitivity. Since the relation between the reactive power and the power angle is not explicit and the optimization periods of different parameters are different, an analytical model of the TS is improved. Considering the impact on the power angle, the indication indices are calculated based on the mean TS and the control parameters, and the set-points of the CCC of the HVDC and the excitation system of the SC to be optimized are determined. The gradients of the objective function are extended to derive a coordinated multiparameter optimization model. The numerical results validate the accuracy and the suppression effect of the proposed models.

The prime contributions of this work are summarized as follows:

(1) A new coordinated optimization to the HVDC and the SC is proposed to suppress the angular oscillations.

(2) An improved analytical expression of the trajectory sensitivity is newly derived and can be used for the optimization of multiple parameters with different periods of optimization.

(3) The applicability of the proposed optimization for different fault scenarios is verified by introducing the index of the importance degree of the node.

(4) The coordinated optimization can reduce the adjustment range of set-points for HVDC, which is safer for the HVDC than the independent optimization without the SC.

The following of this paper is arranged as follows. In Section 2, the relation of the reactive power of the SC with the power angles is validated, which is the basis for

optimizing the control parameters and the set-points of the SC. In Section 3, an improved TS model including the relation between the control parameters and the set-points of the SC and the power angles of the SGs and allowing different optimization periods for the parameters is proposed. In Section 4, an optimization model based on coordinating the control parameters and the set points of the HVDC and the SC is proposed to suppress the oscillations in the AC/HVDC power system. In Section 5, the case studies and analysis are given to validate the accuracy of the improved trajectory sensitivity and the suppression effect with the optimization model. In Section 6, some conclusions are given.

2. Impact of the Reactive Power on the Power Angle Stability

2.1. Effect of the Reactive Power on the Voltage and the Active Power. The power flow of the AC/HVDC system is solved with (1) iteratively, where $\mathbf{P} = [\mathbf{P}_{AC}, \mathbf{P}_{AC\text{-}DC}]$, $\mathbf{Q} = [\mathbf{Q}_{AC}, \mathbf{Q}_{AC\text{-}DC}]$, $\boldsymbol{\theta} = [\boldsymbol{\theta}_{AC}, \boldsymbol{\theta}_{AC\text{-}DC}]$, $\mathbf{V} = [\mathbf{V}_{AC}, \mathbf{V}_{AC\text{-}DC}]$, $\mathbf{P}$ is the active power, $\mathbf{Q}$ is the reactive power, $\mathbf{V}$ is the voltage magnitude, and $\boldsymbol{\theta}$ is the voltage angle. $\mathbf{H}$, $\mathbf{N}$, $\mathbf{M}$, and $\mathbf{L}$ are the sub-Jacobian matrixes. Δ denotes the increment.

$$\begin{bmatrix} \Delta\mathbf{P} \\ \Delta\mathbf{Q} \end{bmatrix} = \begin{bmatrix} \mathbf{H} & \mathbf{N} \\ \mathbf{M} & \mathbf{L} \end{bmatrix} \begin{bmatrix} \Delta\boldsymbol{\theta} \\ \Delta\mathbf{V} \end{bmatrix}. \tag{1}$$

By eliminating the first row, the sensitivity of the voltage with respect to the reactive power is obtained in the following equation. Taking the same increment in the reactive power, the relative voltage sensitivity SRV is given by (3).

$$\frac{\partial \mathbf{V}}{\partial \mathbf{Q}} = \left(\mathbf{L}\text{-}\mathbf{M}\mathbf{H}^{-1}\mathbf{N}\right)^{-1}, \tag{2}$$

$$\begin{aligned} S_{\mathrm{RV}i,j} &= \frac{\Delta V_i}{\Delta V_j} \\ &= \frac{\partial V_i/\partial Q_i}{\partial V_j/\partial Q_j}. \end{aligned} \tag{3}$$

After a fault in the system, the voltage change of the short-circuit bus ΔV_{Fau}, is used as the reference to calculate the voltage of the other buses based on the $S_{\mathrm{RV}i,\mathrm{Fau}}$.

$$\Delta V_i = \Delta V_{\mathrm{Fau}} \times S_{\mathrm{RV}i,\mathrm{Fau}}. \tag{4}$$

The transmission power of the HVDC is reduced and the reactive power of the AC buses is changed after the DC blocking. Considering the change of the bus voltage and the power, (5) is derived from (1). The bus voltage and the active power jointly affect the reactive power. When the reactive power support is not enough, the voltage may be deteriorated and the power flow may be limited.

$$\Delta\mathbf{Q} = \mathbf{M}\mathbf{H}^{-1}\Delta\mathbf{P} + \left(\mathbf{L} - \mathbf{M}\mathbf{H}^{-1}\mathbf{N}\right)\Delta\mathbf{V}. \tag{5}$$

2.2. Effect of the Reactive Power on the Power Angle. To analyze the effect of the reactive power output of the SC (Q_{SC}) on the power angle, (1) is extended by taking the node of SC as the PQ node to obtain the sensitivities of the voltage magnitude and angle of generator bus (V_G and θ_G) to Q_{SC}, which are used as an intermediate quantity to indirectly obtain the sensitivity of the power angle to Q_{SC}. As is known, the power angle can be defined by the following equation:

$$\delta = \arctan\left(\frac{V_{\mathrm{Gy}} + X_q I_{\mathrm{Gx}} + R_s I_{\mathrm{Gy}}}{V_{\mathrm{Gy}} + R_s I_{\mathrm{Gx}} - X_q I_{\mathrm{Gy}}}\right), \tag{6}$$

where I is the current, R is the resistance, and X is the reactance. The subscript G denotes SG, x and y denote axis x and axis y, q denotes quadrature axis, and s denotes the stator.

Considering that Q_{SC} is not included in (6), the derivative method for the compound function is used to derive the sensitivities of V_{Gx}, V_{Gy}, I_{Gx}, and I_{Gy} *to* Q_{SC}. V_{Gx} and V_{Gy} are decided by V_G and θ_G, so the sensitivities of the former to Q_{SC} may be derived from the sensitivities of the latter to Q_{SC} in (7). The sensitivities of the bus injection current, I_{Gx} and I_{Gy}, to Q_{SC} are given in (8), where Y is the admittance matrix.

$$\begin{cases} \dfrac{\partial V_{\mathrm{Gx}}}{\partial Q_{\mathrm{SC}}} = \cos\,\theta_G \dfrac{\partial V_G}{\partial Q_{\mathrm{SC}}} + V_G \dfrac{\partial \cos\,\theta_G}{\partial Q_{\mathrm{SC}}}, \\ \dfrac{\partial V_{\mathrm{Gy}}}{\partial Q_{\mathrm{SC}}} = \sin\,\theta_G \dfrac{\partial V_G}{\partial Q_{\mathrm{SC}}} + V_G \dfrac{\partial \sin\,\theta_G}{\partial Q_{\mathrm{SC}}}, \end{cases} \tag{7}$$

$$\begin{bmatrix} \dfrac{\partial I_{\mathrm{Gx}}}{\partial Q_{\mathrm{SC}}} \\ \dfrac{\partial I_{\mathrm{Gy}}}{\partial Q_{\mathrm{SC}}} \end{bmatrix} = \begin{bmatrix} \dfrac{\partial V_{\mathrm{Gx}}}{\partial Q_{\mathrm{SC}}} & -\dfrac{\partial V_{\mathrm{Gy}}}{\partial Q_{\mathrm{SC}}} \\ \dfrac{\partial V_{\mathrm{Gy}}}{\partial Q_{\mathrm{SC}}} & \dfrac{\partial V_{\mathrm{Gx}}}{\partial Q_{\mathrm{SC}}} \end{bmatrix} \begin{bmatrix} \mathrm{Re}(Y) \\ \mathrm{Im}(Y) \end{bmatrix} + \begin{bmatrix} \dfrac{\partial \mathrm{Re}(Y)}{\partial Q_{\mathrm{SC}}} & -\dfrac{\partial \mathrm{Im}(Y)}{\partial Q_{\mathrm{SC}}} \\ \dfrac{\partial \mathrm{Im}(Y)}{\partial Q_{\mathrm{SC}}} & \dfrac{\partial \mathrm{Re}(Y)}{\partial Q_{\mathrm{SC}}} \end{bmatrix} \begin{bmatrix} V_{\mathrm{Gx}} \\ V_{\mathrm{Gy}} \end{bmatrix}. \tag{8}$$

With the partial derivative of (6) to Q_{SC}, the sensitivity of the power angle to Q_{SC} is obtained in the following equation:

$$\frac{\partial\delta}{\partial Q_{SC}} = \frac{\partial\delta}{\partial V_{Gx}}\frac{\partial V_{Gx}}{\partial Q_{SC}} + \frac{\partial\delta}{\partial V_{Gy}}\frac{\partial V_{Gy}}{\partial Q_{SC}} + \frac{\partial\delta}{\partial I_{Gx}}\frac{\partial I_{Gx}}{\partial Q_{SC}} + \frac{\partial\delta}{\partial I_{Gy}}\frac{\partial I_{Gy}}{\partial Q_{SC}}. \tag{9}$$

By substituting (1), (5), (7), and (8) into (9), it is found that the active and reactive power interacts with the bus voltage, which together affects the power angle. The relation of the reactive power of the SC and the power angle is validated and the coordinated optimization to the HVDC and the SC may be introduced to improve the power angular oscillations.

3. The Improved Trajectory Sensitivity considering Different Periods of Optimization

3.1. Dynamic Modeling of the AC/HVDC Power System. In this paper, the SGs adopt the 12th order model, including the electromagnetic equation (the 3rd order), the motion equation (the 2nd order), the governor (the 3rd order), and the excitation system (the 4th order). The model of the SC is based on [35], and it includes the electromagnetic equation (the 3rd order), the motion equation (the 2nd order), and the excitation system (the 4th order), and the excitation system (the 4th order). Figure 1 shows the model of the SC, where K_A and T_A are the gain and the time constant of the main regulator, K_F and T_F are the gain and the time constant of the rate feedback, V_{ref} is the exciter reference voltage, V_{f0} is the initial value of the output voltage of the exciter, and V_M, V_A, V_E, and V_F are the voltage outputs of the measurement, the main regulator, the exciter, and the rate feedback, respectively. The model of the HVDC is described in [36], where the CCC is applied to the rectifier and the constant extinction angle (CEA) is applied to the inverter [37]. Figure 2 shows the model of the HVDC, where k_{pr} and k_{ir} are PI parameters of the CCC, $I_{DC,ref}$, and α_{ref} are the references for the direct current and the firing-delayed angle.

3.2. Improved Analytical Expression of TS in the AC/HVDC Power System. To solve the problem that the trajectory sensitivities of system variables are often found with respect to control parameters instead of set-points without considering different periods of optimization, the improved TS is newly derived as follows. The flowchart of the adjustment of control parameters and set-points is shown in Figure 3, where the fault occurs at t_1, the control parameters are adjusted to the optimal values at the beginning of the time-domain simulation, and the set-points are adjusted at t_2 and restored to the initial valves at t_3.

The time-domain simulation is based on the differential-algebraic equations (DAE) of the AC/HVDC power system in (10), where f, g, x, and y are the differential equations, algebraic equations, state variables, and algebraic variables, respectively, a is the system parameter and t is the time. The subscript 0 denotes the initial value, cp denotes the control parameter, and sp denotes the set-point.

$$\begin{cases} \dot{x} = f\big(x(t), y(t), a_{cp}, a_{sp}\big), \\ 0 = g\big(x(t), y(t), a_{cp}, a_{sp}\big), \\ x(t_0) = x_0, \\ y(t_0) = y_0. \end{cases} \tag{10}$$

a_{cp} and a_{sp} are taken as variables during their respective optimization periods and constants during the rest of the time. Because of different periods of optimization to a_{cp} and a_{sp}, the partial derivative equations of (10) to a_{cp} are different from that to a_{sp}. Compared with (11), the step function ε is introduced in (12) to differentiate periods of optimization.

$$\begin{cases} \dot{x}_{a_{cp}} = f_x x_{a_{cp}} + f_y y_{a_{cp}} + f_{a_{cp}}, \\ 0 = g_x x_{a_{cp}} + g_y y_{a_{cp}} + g_{a_{cp}}, \end{cases} \tag{11}$$

$$\begin{cases} \dot{x}_{a_{sp}} = f_x x_{a_{sp}} + f_y y_{a_{sp}} + f_{a_{sp}}\big[\varepsilon(t-t_2) - \varepsilon(t-t_3)\big], \\ 0 = g_x x_{a_{sp}} + g_y y_{a_{sp}} + g_{a_{sp}}\big[\varepsilon(t-t_2) - \varepsilon(t-t_3)\big], \end{cases} \tag{12}$$

where f_x, f_y, f_{acp}, f_{asp}, g_x, g_y, g_{acp}, and g_{asp} are the time-varying matrices for the partial derivative.

Considering that multiple state variables are coupled in (11) and (12), the intermediate variables are introduced to decouple state variables. The decoupling process for the SC is given as an example. The intermediate variables ϕ_{ITM1} and ϕ_{ITM2} are defined as follows:

$$\begin{cases} \phi_{ITM1} = T_{d0}''\big(E_q'' - E_q'\big), \\ \phi_{ITM2} = K_F V_E - T_F V_F, \end{cases} \tag{13}$$

where T_{d0}'' is the d-axis subtransient open-circuit time constant, E_q'' is the q-axis subtransient electromotive force, E_q' is the q-axis transient electromotive force.

The partial derivative equations of (13) with respect to a parameter to be optimized α are given in the following equation:

$$\begin{cases} 0 = \phi_{ITM1,\alpha} - T_{d0}''\big(E_{q\alpha}'' - E_{q\alpha}'\big), \\ 0 = \phi_{ITM2,\alpha} - K_F V_{E\alpha} + T_F V_{F\alpha}, \end{cases} \tag{14}$$

combining (13), and the electromagnetic equation and the excitation system model of the SC, the newly derivative equations are given in (15). With the help of the intermediate variables, each row has only one state variable, i.e., the differential equations and the state variables are decoupled.

$$\begin{cases} \dfrac{d\phi_{ITM1}}{dt} = E_q' - E_q'' - \big(X_d' - X_d''\big) I_d, \\ \dfrac{d\phi_{ITM2}}{dt} = V_F, \end{cases} \tag{15}$$

where X_d' is the d-axis transient reactance, X_d'' is the d-axis subtransient reactance, and I_d is the d-axis current component.

All state variables of the system, including the added intermediate variables, are rowed into the diagonal matrix, the trajectory sensitivities are decoupled, and the Jacobi matrices of state variables and algebraic variables are in the upper and lower parts of the matrix, respectively. By applying the trapezoidal differentiation method for (14) and (15) with the intermediate variables, the analytical expressions of the trajectory sensitivity are newly given in (16) and (17), where U is the unit matrix, and the superscripts t and $t-1$ denote the current and last moment, respectively. The right-most term is the imbalanced matrix. Most of its elements are 0, except for those with a_{cp} or a_{sp}.

$$\begin{bmatrix} x_{a_{\mathrm{cp}}}^{(t)} \\ y_{a_{\mathrm{cp}}}^{(t)} \end{bmatrix} = \begin{bmatrix} \frac{2U}{\Delta t} - f_x^{(t)} & -f_x^{(t)} \\ g_y^{(t)} & g_y^{(t)} \end{bmatrix}^{-1} \times \left(\begin{bmatrix} \frac{2U}{\Delta t} + f_x^{(t-1)} & f_y^{(t-1)} \\ 0 & 0 \end{bmatrix} \times \begin{bmatrix} x_{a_{\mathrm{cp}}}^{(t-1)} \\ y_{a_{\mathrm{cp}}}^{(t-1)} \end{bmatrix} + \underbrace{\begin{bmatrix} -f_{a_{\mathrm{cp}}}^{(t)} \\ -g_{a_{\mathrm{cp}}}^{(t)} \end{bmatrix}}_{\mathrm{Imbalabcedmatrix}} \right), \tag{16}$$

$$\begin{bmatrix} x_{a_{\mathrm{sp}}}^{(t)} \\ y_{a_{\mathrm{sp}}}^{(t)} \end{bmatrix} = \begin{bmatrix} \frac{2U}{\Delta t} - f_x^{(t)} & -f_y^{(t)} \\ g_x^{(t)} & g_y^{(t)} \end{bmatrix}^{-1} \times \left(\begin{bmatrix} \frac{2U}{\Delta t} + f_x^{(t-1)} & f_y^{(t-1)} \\ 0 & 0 \end{bmatrix} \times \begin{bmatrix} x_{a_{\mathrm{sp}}}^{(t-1)} \\ y_{a_{\mathrm{sp}}}^{(t-1)} \end{bmatrix} + \underbrace{\begin{bmatrix} -f_{a_{\mathrm{sp}}}^{(t)} \left[\varepsilon(t-t_2) - \varepsilon(t-t_3) \right] \\ -g_{a_{\mathrm{sp}}}^{(t)} \left[\varepsilon(t-t_2) - \varepsilon(t-t_3) \right] \end{bmatrix}}_{\mathrm{Imbalancedmatrix}} \right). \tag{17}$$

By modifying the imbalanced matrix and the step function in (17), trajectory sensitivities of system variables to set-points are calculated during the optimization period. After set-points are restored to the initial value, elements of the imbalanced matrix are 0, while those of the TS are not 0 and the subsequent effect of the optimization is still quantified. Some nonzero elements in the imbalanced matrix are given in (18) and (19).

The nonzero elements e corresponding to the control parameters of the SC and the CCC are given in the following equation:

$$\begin{cases} e_{K_A} = -\dfrac{0.5\left(V_M^{(t)} + V_F^{(t)} + V_M^{(t-1)} + V_F^{(t-1)}\right) - V_{\mathrm{ref}}}{T_A}, \\ e_{T_A} = \dfrac{0.5\left[V_A^{(t)} + V_A^{(t-1)} + K_A\left(V_M^{(t)} + V_F^{(t)} + V_M^{(t-1)} + V_F^{(t-1)} + V_{\mathrm{ref}}\right)\right]}{T_{\mathrm{A}}^2}, \\ e_{K_F} = V_E^{(t)}, \\ e_{T_F} = -V_F^{(t)}, \\ e_{K_{\mathrm{pr}}} = -\left(I_{\mathrm{DC,ref}} - I_{\mathrm{DC}}^{(t)}\right), \\ e_{K_{\mathrm{ir}}} = -\left[0.5\left(I_{\mathrm{DC}}^{(t)} + I_{\mathrm{DC}}^{(t-1)}\right) - I_{\mathrm{DC,ref}}\right]. \end{cases} \tag{18}$$

The nonzero elements corresponding to the set-points are given in the following equation:

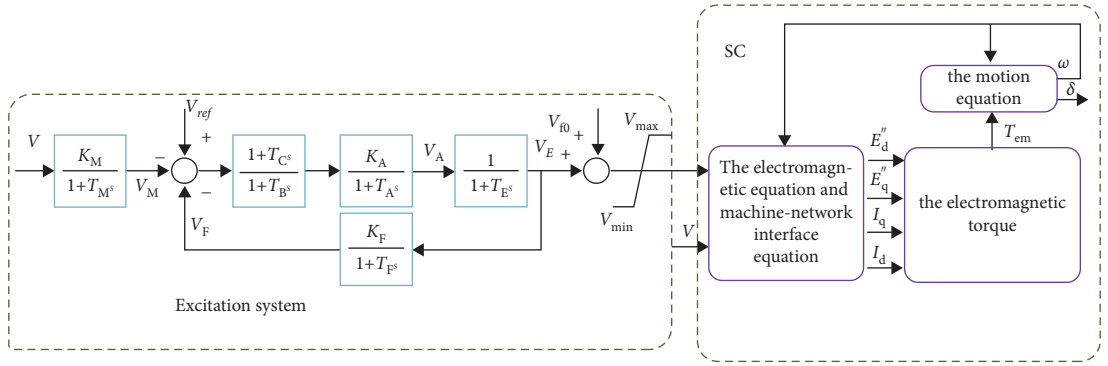

Figure 1: Model of SC.

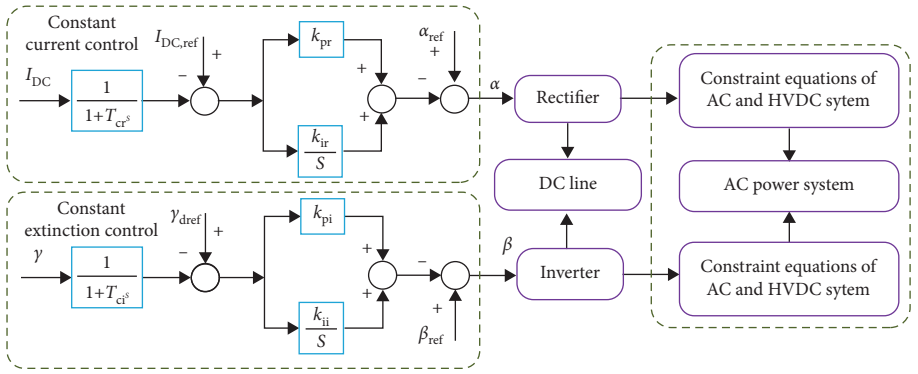

Figure 2: HVDC transmission system.

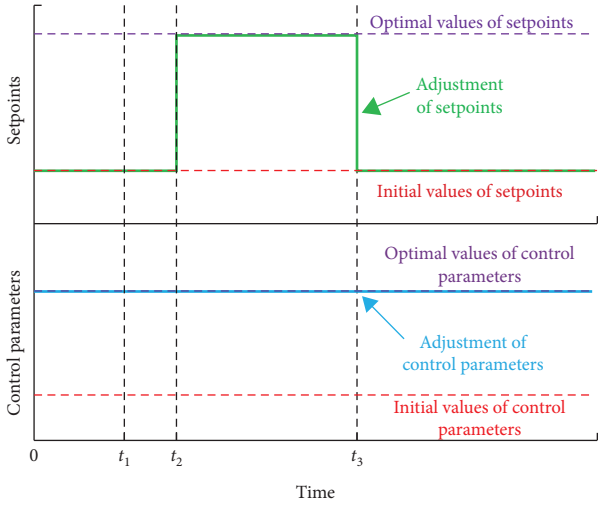

Figure 3: Adjustment of control parameters and set-points with different periods.

$$\begin{cases} e_{V_{\text{ref}}} = \dfrac{K_A[\varepsilon(t-t_2)-\varepsilon(t-t_3)]}{T_A}, \\ e_{V_{f0}} = -[\varepsilon(t-t_2)-\varepsilon(t-t_3)], \\ e_{\alpha_{\text{ref}}} = -[\varepsilon(t-t_2)-\varepsilon(t-t_3)], \\ e_{I_{\text{DC,ref}}} = K_{\text{ir}}[\varepsilon(t-t_2)-\varepsilon(t-t_3)]. \end{cases} \tag{19}$$

It is worth noting that the matrices f_x, f_y, g_x, and g_y in (16) and (17) are the same as those in (10). Consequently, (16) and (17) are easy to be built up after one simulation just with modifying the imbalanced matrices, which are computationally more economical than the perturbation method. The expressions of f_x and f_y are given in (20) and (21). g_x and g_y are derived similarly.

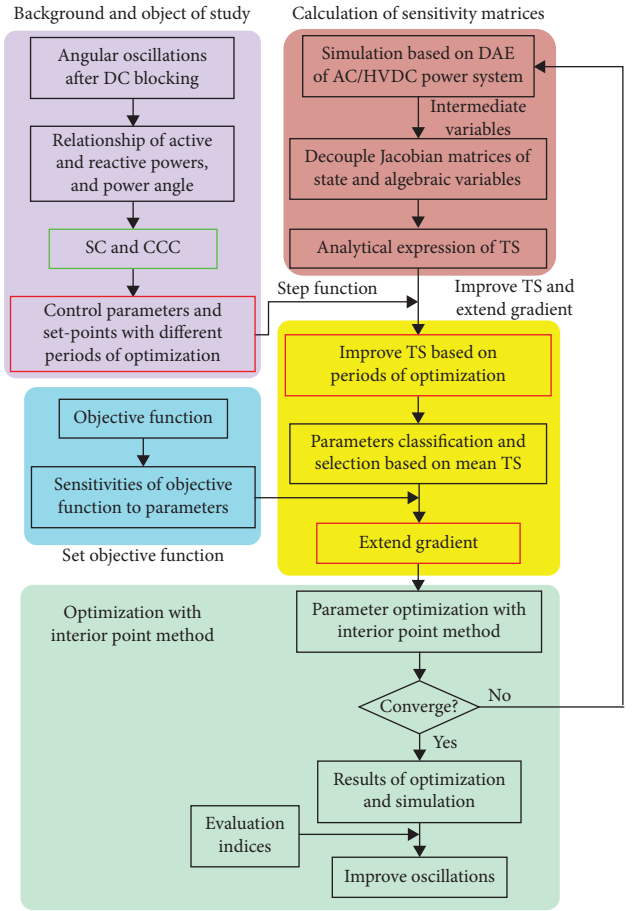

FIGURE 4: Multiparameter coordinated optimization differentiating the period of optimization.

$$f_x = \begin{bmatrix} f_{\mathrm{SGx_{SG}}} & f_{\mathrm{SGx_{SC}}} & f_{\mathrm{SGx_{HVDC}}} \\ f_{\mathrm{SCx_{SG}}} & f_{\mathrm{SCx_{SC}}} & f_{\mathrm{SCx_{HVDC}}} \\ f_{\mathrm{HVDCx_{SG}}} & f_{\mathrm{HVDCx_{SC}}} & f_{\mathrm{HVDCx_{HVDC}}} \end{bmatrix}, \tag{20}$$

$$f_y = \begin{bmatrix} f_{\mathrm{SGy_{SG}}} & f_{\mathrm{SGy_{SC}}} & f_{\mathrm{SGy_{HVDC}}} \\ f_{\mathrm{SCy_{SG}}} & f_{\mathrm{SCy_{SC}}} & f_{\mathrm{SCy_{HVDC}}} \\ f_{\mathrm{HVDCy_{SG}}} & f_{\mathrm{HVDCy_{SC}}} & f_{\mathrm{HVDCy_{HVDC}}} \end{bmatrix}. \tag{21}$$

4. Coordinate Optimization Model and Solution Algorithm

4.1. Selecting the Parameters to be Optimized Based on the Sensitivity Evaluation Index. The parameters to be optimized are selected by the evaluation index of the TS. To eliminate the difference in the range and the dimension of parameters, the mean TS is introduced [28], which reflects the influence degree of parameters on the dynamic process.

$$S_{\mathrm{mean}} = \frac{1}{\mathrm{NUM_{samp}}} \sum_{i=1}^{\mathrm{NUM_{samp}}} \left| \frac{\partial [p(\alpha, i)/p_0]}{\partial [\alpha/\alpha_0]} \right|, \tag{22}$$

where S_{mean} is the value of the mean TS, p is one of system variables, and $\mathrm{NUM_{samp}}$ is the sampling number on the TS curves.

4.2. The Optimization Model. Taking the power angle of the #N SG as the reference, the objective function J is established in (23) by calculating the difference-squared integral of the power angle difference in the transient process and the steady-state power angle difference after the fault.

$$\min J = \sum_{\substack{j=1 \\ j \neq N}}^{\mathrm{NUM_{SG}}} \int_0^{t_{\mathrm{end}}} \left[\left(\frac{\delta_{j,N}(t) - \delta_{j,N}(t_{\mathrm{end}})}{\delta_{j,N}(t_{\mathrm{end}})} \right)^2 \right] \mathrm{d}t, \tag{23}$$

$$\begin{cases} \delta_{j,N}(t) = \delta_j(t) - \delta_N(t), \\ \delta_{j,N}(t_{\mathrm{end}}) = \delta_j(t_{\mathrm{end}}) - \delta_N(t_{\mathrm{end}}), \end{cases} \tag{24}$$

where $\mathrm{NUM_{SG}}$ is the number of SGs, and t_{end} is the finish time of the simulation, δ_j is the power angle of the #j SG, and $\delta_{j,N}$ is the power angle difference between the #j and the #N SGs.

Considering equality and inequality constraints, the optimization model is proposed in (25), where $a^{\min}$ and $a^{\max}$ are the upper and lower limits of parameters.

$$\begin{cases} \min J, \\ \text{s.t.} \quad \dot{x} = f(x(t), y(t), a), \\ 0 = g(x(t), y(t), a), \\ a = [a_{cp}\, a_{sp}], \\ a^{\min} \le a \le a^{\max}. \end{cases} \tag{25}$$

4.3. Multiparameter Coordinated Optimization considering the Optimization Period. Considering the nonlinearity of the model in (25) and the advantage of the direct optimization, the interior point method is introduced, which requires the first-order and second-order gradient information of the objective function. By accumulating the TS of the objective function J to a, the first-order gradient is obtained by (26), where $\mathrm{NUM_{ste}}$ is the number of the simulation steps and $S_{\delta_j(t_m),a}$ is the TS of the power angle of the #j SG to a at the m^{th} step.

$$\frac{\partial J}{\partial \mathbf{a}} = 2\Delta t \sum_{m=0}^{\mathrm{NUM_{ste}}} \sum_{\substack{j=1 \\ j \neq N}}^{\mathrm{NUM_{SG}}} \frac{\delta_{j,N}(t_m) - \delta_{j,N}(t_{\mathrm{NUM_{ste}}})}{\delta_{j,N}(t_{\mathrm{NUM_{ste}}})^2} S_{\delta_{j,N}(t_m),a}, \tag{26}$$

$$S_{\delta_{j,N}(t_m),\mathbf{a}} = S_{\delta_{j,N}(t_m),\mathbf{a}} - S_{\delta_{j,N}(t_m),\mathbf{a}}. \tag{27}$$

Considering that the first-order gradient in (26) is not suitable for difference periods of multiple parameters, this paper proposes the extended first-order gradient with the improved TS in (28) and (29).

$$\begin{bmatrix} \dfrac{\partial \mathbf{J}}{\partial \mathbf{a}_{cp}} \\ \dfrac{\partial \mathbf{J}}{\partial \mathbf{a}_{sp}} \end{bmatrix} = 2\Delta t \sum_{m=0}^{\mathrm{NUM}_{ste}} \sum_{\substack{j=1 \\ j \neq N}}^{\mathrm{NUM}_{\mathrm{SG}}} \frac{\delta_{j,N}(t_m) - \delta_{j,N}\left(t_{\mathrm{NUM}_{ste}}\right)}{\delta_{j,N}\left(t_{\mathrm{NUM}_{ste}}\right)^2} \begin{bmatrix} \mathbf{S}_{\delta_{j,N}(t_m),\mathbf{a}_{cp}} \\ \mathbf{S}_{\delta_{j,N}(t_m),\mathbf{a}_{sp}} \end{bmatrix}, \tag{28}$$

$$\begin{bmatrix} \mathbf{S}_{\delta_{j,N}(t_m),\mathbf{a}_{\mathrm{cp}}} \\ \mathbf{S}_{\delta_{j,N}(t_m),\mathbf{a}_{\mathrm{sp}}} \end{bmatrix} = \begin{bmatrix} \mathbf{S}_{\delta_j(t_m),\mathbf{a}_{cp}} \\ \mathbf{S}_{\delta_j(t_m),\mathbf{a}_{sp}} \end{bmatrix} - \begin{bmatrix} \mathbf{S}_{\delta_N(t_m),\mathbf{a}_{cp}} \\ \mathbf{S}_{\delta_N(t_m),\mathbf{a}_{sp}} \end{bmatrix}. \tag{29}$$

Since the objective function is nonlinear, the Jacobian and Hessian matrices are to be defined for optimization by the interior point method. The calculation of the Hessian matrix needs a lot of storage and calculation effort. Hence the BFGS algorithm is used to derive the approximate form of the Hessian matrix in an iterative manner in (30), where $g_k = [\partial J/\partial a_{\mathrm{cp},k}, \partial J/\partial a_{\mathrm{sp},k}]$, $m_k = g_k - g_{k-1}$, $u_k = a_k - a_{k-1}$, and k is the iteration number.

$$G_k = G_{k-1} + \frac{m_k m_k^T}{m_k^T m_k} - \frac{G_{k-1} u_k u_k^T G_{k-1}}{u_k^T G_{k-1} u_k}. \tag{30}$$

4.4. The Evaluation Indices for the Optimization Effect. To evaluate the optimization effect, 3 indices are defined,

(a) The optimization ratio of the amplitudes of the peak and the trough λ_{apt}

The steady-state value of the power angle difference $\delta(t_{\mathrm{end}})$ after the fault is taken as the reference, the average amplitude of peak and trough of the power angle difference δ_{apt} is defined as follows:

$$\delta_{\mathrm{apt}} = \frac{1}{\mathrm{NUM}_{pk} + \mathrm{NUM}_{tr}} \left(\sum_{i=1}^{\mathrm{NUM}_{pk}} \left| \delta_{i,pk} - \delta(t_{\mathrm{end}}) \right| + \sum_{j=1}^{\mathrm{NUM}_{tr}} \left| \delta_{j,tr} - \delta(t_{\mathrm{end}}) \right| \right), \tag{31}$$

where $\mathrm{NUM}_{\mathrm{pk}}$ is the number of the peak, $\mathrm{NUM}_{\mathrm{tr}}$ is the number of the trough, $\delta_{i,\mathrm{pk}}$ is the angle of the i^{th} peak, and $\delta_{j,\mathrm{tr}}$ is the angle of the j^{th} trough.

λ_{apt} is defined by (32), where $\delta_{\mathrm{apt,woop}}$ is the average amplitude of peak and trough of the power angle difference without optimization, and $\delta_{\mathrm{apt,wop}}$ is that with optimization.

$$\lambda_{\mathrm{apt}} = \frac{\delta_{\mathrm{apt,woop}} - \delta_{\mathrm{apt,wop}}}{\delta_{\mathrm{apt,woop}}} \times 100\%. \tag{32}$$

(b) The optimization ratio of the convergence time λ_{cv}

By taking ±5% of $\delta(t_{\mathrm{end}})$ as the convergence range, and $t_{\mathrm{cv,woop}}$ is the convergence time without optimization and $t_{\mathrm{cv,wop}}$ is that with optimization, and λ_{cv} is obtained in .

$$\lambda_{\mathrm{cv}} = \frac{t_{\mathrm{cv,woop}} - t_{\mathrm{cv,wop}}}{t_{\mathrm{cv,woop}}} \times 100\%. \tag{33}$$

(c) The optimization ratio of the objective function value λ_J

To describe the suppression effect of the proposed optimization during the whole transient process, λ_J is defined with the objective function value without optimization J_{woop} and that with optimization J_{wop} in the following equation:

$$\lambda_J = \frac{J_{\mathrm{woop}} - J_{\mathrm{wop}}}{J_{\mathrm{woop}}} \times 100\%. \tag{34}$$

4.5. Procedure of Optimization. Considering the relation of active power, reactive power, and power angle, it may improve the angular oscillations by optimizing control parameters and set-points of the HVDC and the SC based on the improved TS. The multiparameter coordinated optimization scheme differentiating the periods of optimization is shown in Figure 4, where the words in the green font show the optimization objects and the words in the red font show the difficulties of the proposed scheme.

The elaborate description of the optimization procedures is as follows:

Firstly, based on the differential-algebraic equations of the AC/HVDC power system in (10), the trajectory sensitivities with respect to all control parameters and set-points are obtained by the time-domain simulation and the improved analytical expression of TS, as shown in (11) and (12).

Secondly, the control parameters and set-points to be optimized are selected based on the mean trajectory sensitivities in (22).

Thirdly, based on (28) and (30), the first-order and second-order gradient information of the objective function with respect to the control parameters and the set-points to be optimized is extended, which is required by the interior point method.

Fourthly, with the gradient information, the optimization model in (25) is solved by the interior point method, and the optimal values of the control parameters and the set-points are obtained.

Fifthly, the duality gap of the interior point method is checked. If the duality gap is smaller than the convergence value, which is set at 10^{-4} in this paper, the optimization procedures are completed. Otherwise, it returns to the first step, and the next literation continues.

4.6. Parameter Optimization under Scenarios with Different Faults. The optimization results for a single fault are difficult to achieve for all faults, and even the postfault response is degraded in some scenarios. To improve the applicability, the weighting value of the optimization results a' is derived as follows: By introducing the index of the importance degree of the node φ_{IDN} [38], the severity index of the nth scenario $\varphi_{\mathrm{SEV}}(n)$ is calculated in the following equation:

$$\varphi_{\mathrm{SEV}}(n) = \frac{\varphi_{\mathrm{IDN}}(n)}{\sum_{i\in\Omega}\varphi_{\mathrm{IDN}}(i)}, \tag{35}$$

where Ω is the set of the scenarios, $\varphi_{\mathrm{IDN}}(n)$ is the index of the importance degree of the fault bus in the nth scenario.

By accumulating the optimization results under different scenarios with the severity index, a' is obtained in (36), where $a_{n,op}$ is the optimization results for the nth scenario.

$$\mathbf{a}' = \sum_{n\in\Omega} \varphi_{\mathrm{SEV}}(n)\mathbf{a}_{n,op}. \tag{36}$$

Considering the hazard level of different faults and introducing the weighting value of the optimization results to the proposed scheme may improve its applicability for different faults.

It should be noted that the proposed models are based on a given system state, but the system scenarios and fault conditions are always changing. To improve the feasibility for actual application, the optimized parameters from different states are compromised to derive a comprehensive solution to suppress the angular oscillation. The interior point method is applied to solve the proposed model. Now the heuristic methods are widely used in many existing optimization models to damp the oscillations, which is easy to implement but has drawbacks in terms of computation efficiency and the global solution [39]. Therefore, a direct optimization, e.g., the interior point method, may be more desirable.

5. Numerical Analysis

The program is written by the authors by using MATLAB R2021a language and ran on the computer with Intel Core i5-10400 CPU 2.9 GHz, 16 G. To validate the effectiveness of the proposed models, the IEEE-39-bus in Figure 5 is applied. The AC line 2-3 is replaced with an HVDC line with the loading of 365 MW [40]. The SC is located at bus 2, i.e., the rectifier side. The parameters of the CCC and the CEA are found in [36].

Four scenarios are designed,

Scenario 1. A three-phase short-circuit fault occurs at bus 26 followed by DC mono-pole blocking fault.

Scenario 2. A three-phase short-circuit fault occurs at bus 9 followed by DC mono-pole blocking fault.

Scenario 3. A three-phase short-circuit fault occurs at bus 28 followed by DC mono-pole blocking fault.

Scenario 4. A three-phase short-circuit fault occurs at bus 4 followed by DC mono-pole blocking fault.

The analysis in Sections 5.1 to 5.3 based on Scenario 1 is to validate the effectiveness of the proposed model in the signal scenario, and that in Section 5.4 based on the set of scenarios is to improve the applicability for different faults.

5.1. Validation of the Improved Trajectory Sensitivity. To verify the accuracy of the improved TS, the trajectory sensitivities of δ_1 with respect to K_F and $I_{\mathrm{DC,ref}}$ (S_{δ_1,K_F} and $S_{\delta_1,I_{\mathrm{DC,ref}}}$) are calculated by the analytical method and the perturbation method, respectively. The sensitivity curves are shown in Figures 6 and 7, which almost coincide. Table 1 gives the error analysis of the two methods and shows that the maximum absolute error is only 5.22×10^{-5} and the maximum relative error is only 1.82%. Hence, the accuracy of the improved TS is verified.

5.2. The Critical Parameters Selected with the TS Index. To find the critical control parameters and set-points to be optimized, the evaluation index in Section 4.1 is applied. The control parameters and the set-points of the excitation systems of the SC and the CCC of the HVDC are given in Table 2, along with the evaluation indices for δ_1 with respect to those. The evaluation indices corresponding to K_A, K_F, and T_F, which are 1.27×10^{-2}, 0.98×10^{-2}, and 0.61×10^{-2}, respectively, are the greater ones among the control parameters of the SC and the CCC. The evaluation indices corresponding to V_{ref}, V_{f0}, $I_{\mathrm{DC,ref}}$, and α_{ref} are 5.38×10^{-1}, 1.67×10^{-3}, 2.32×10^{-4}, and 1.56×10^{-1}, respectively. It is clear that the evaluation indices corresponding to V_{ref} and

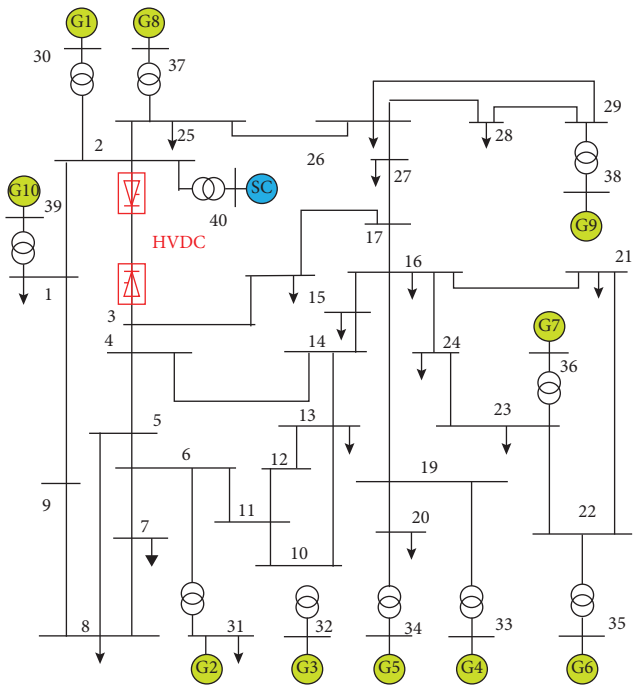

Figure 5: IEEE 39-bus test system with HVDC line.

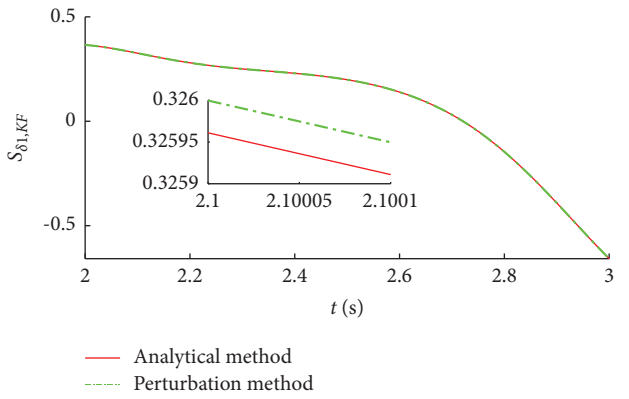

Figure 6: Trajectory sensitivity of the power angle of #1 SG to K_F.

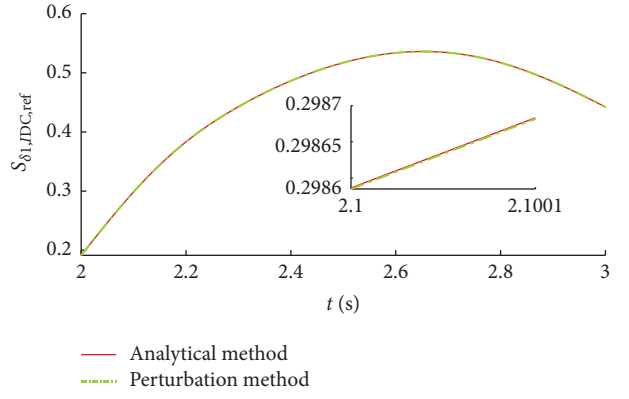

Figure 7: Trajectory sensitivity of the power angle of #1 SG to $I_{DC,ref}$.

Table 1: Error analysis of the improved TS.

Error	Sensitivity	Max	Average
Absolute error	S_{δ_1,K_F}	5.22×10^{-5}	1.47×10^{-5}
	$S_{\delta_1,I_{DC,ref}}$	3.93×10^{-6}	2.21×10^{-6}
Relative error (%)	S_{δ_1,K_F}	1.82	0.14
	$S_{\delta_1,I_{DC,ref}}$	0.26	0.05

Table 2: Calculation of evaluation indices for δ_1 based on TS.

Parameter			S_{mean}
Control parameter	SC	K_A	1.27×10^{-2}
		(T_A)	4.41×10^{-5}
		K_F	0.98×10^{-2}
		T_F	0.61×10^{-2}
	CCC	(K_{pr})	5.24×10^{-5}
		(K_{ir})	4.52×10^{-4}
Set-point	SC	V_{ref}	5.38×10^{-1}
		(V_{f0})	1.67×10^{-3}
	CCC	(α_{ref})	2.32×10^{-4}
		$I_{DC,ref}$	1.56×10^{-1}

Table 3: The TS indices for δ_2 to δ_5.

Parameter	δ_{SG2}	δ_{SG3}	δ_{SG4}	δ_{SG5}
K_A	1.47×10^{-2}	1.47×10^{-2}	1.47×10^{-2}	1.47×10^{-2}
(T_A)	4.83×10^{-5}	5.05×10^{-5}	4.98×10^{-5}	5.11×10^{-5}
K_F	1.14×10^{-2}	1.16×10^{-2}	1.18×10^{-2}	1.21×10^{-2}
T_F	0.64×10^{-2}	0.67×10^{-2}	0.69×10^{-2}	0.71×10^{-2}
(K_{pr})	5.03×10^{-5}	5.02×10^{-5}	5.03×10^{-5}	5.04×10^{-5}
(K_{ir})	4.29×10^{-4}	4.20×10^{-4}	4.16×10^{-4}	4.33×10^{-4}
V_{ref}	5.96×10^{-1}	5.98×10^{-1}	6.03×10^{-1}	6.07×10^{-1}
(V_{f0})	1.69×10^{-3}	1.70×10^{-3}	1.69×10^{-3}	1.71×10^{-3}
(α_{ref})	2.35×10^{-4}	2.35×10^{-4}	2.36×10^{-4}	2.36×10^{-4}
$I_{DC,ref}$	1.60×10^{-1}	1.60×10^{-1}	1.60×10^{-1}	1.60×10^{-1}

$I_{DC,ref}$ are the larger two among all set-points. The evaluation indices for δ_2 to δ_{10} are given in Tables 3 and 4, and the evaluation indices corresponding to K_A, K_F, T_F, V_{ref}, and $I_{DC,ref}$ are greater than others. So K_A, K_F, and T_F are selected as the critical control parameters, and V_{ref} and $I_{DC,ref}$ are selected as the critical set-points. The control parameters and the set-points marked by the ( ) are not to be optimized in Tables 2–4.

5.3. Suppression to the Oscillations in the Signal Scenario. In this section, different optimization cases are designed,

Case 1. Optimization to $I_{DC,ref}$.

Case 2. Optimization to V_{ref} and $I_{DC,ref}$.

Case 3. Optimization to K_A, K_F, and T_F.

Case 4. Optimization to K_A, K_F, T_F, and V_{ref}.

Table 4: The TS indices for δ_6 to δ_{10}.

Parameter	δ_{SG6}	δ_{SG7}	δ_{SG8}	δ_{SG9}	δ_{SG10}
K_A	1.47×10^{-2}	1.48×10^{-2}	1.34×10^{-2}	1.44×10^{-2}	1.41×10^{-2}
(T_A)	4.87×10^{-5}	5.27×10^{-5}	4.41×10^{-5}	4.45×10^{-5}	4.22×10^{-5}
K_F	1.16×10^{-2}	1.25×10^{-2}	0.78×10^{-2}	0.98×10^{-2}	0.87×10^{-2}
T_F	0.68×10^{-2}	0.73×10^{-2}	0.49×10^{-2}	0.56×10^{-2}	0.52×10^{-2}
(K_{pr})	5.06×10^{-5}	5.03×10^{-5}	5.17×10^{-5}	5.03×10^{-5}	5.11×10^{-5}
(K_{ir})	4.20×10^{-4}	4.29×10^{-4}	4.21×10^{-4}	4.20×10^{-4}	4.14×10^{-4}
V_{ref}	6.01×10^{-1}	6.11×10^{-1}	5.44×10^{-1}	5.67×10^{-1}	5.62×10^{-1}
(V_{f0})	1.71×10^{-3}	1.69×10^{-3}	1.69×10^{-3}	1.69×10^{-3}	1.69×10^{-3}
(α_{ref})	2.36×10^{-4}	2.37×10^{-4}	2.31×10^{-4}	2.33×10^{-4}	2.32×10^{-4}
$I_{DC,ref}$	1.59×10^{-1}	1.61×10^{-1}	1.56×10^{-1}	1.57×10^{-1}	1.57×10^{-1}

Table 5: The initial values and ranges of the parameters.

Parameter	Initial value	Range
K_A	200	[100, 400]
K_F	1	[0.5, 0.5]
T_F (s)	0.1	[0.05, 0.5]
V_{ref} (p.u.)	1.0484	[0.9, 1.1]
$I_{DC,ref}$ (p.u.)	0.9125	[0.85, 1]

Table 6: Effect analysis of optimization to $I_{DC,ref}$.

	$\delta_{apt,woop}$ (°)	$\delta_{apt,wop}$ (°)	λ_{apt} (%)
$\delta_{2,1}$	5.24	5.16	1.53
$\delta_{5,1}$	5.90	5.77	2.06
	J_{woop}	J_{wop}	λ_J(%)
	40.44	39.77	1.66

Case 5. Optimization to K_A, K_F, T_F, V_{ref}, and $I_{DC,ref}$ (the optimization scheme proposed by this paper).

Cases 1 and 2 are compared to reflect the suppression effect of the SC on the angular oscillations and the effectiveness of coordination optimization for active power and reactive power. The comparison of Cases 2 and 3 is to investigate the difference between optimization to control set-points and optimization to control parameters. By designing different optimization cases, the effectiveness of the proposed optimization is verified.

The initial values are shown in Table 5. Considering the time delay of the fault diagnosis, the stability control device, and the adjustment to the parameters in the actual engineering [41, 42], the adjustment of set-points starts at 70 ms after the DC blocking and continues for 1 s before returning to the initial value. In order to illustrate the optimization effect of parameters with small sensitivities, the optimization to K_{pr} and K_{ir} of the CCC is designed in Section 5.3.6.

5.3.1. Optimization to $I_{DC,ref}$. Considering the short-time overload capability of the nonfault pole, the upper limit of $I_{DC,ref}$ is set to 1 p.u. [33]. Keeping other parameters constant, $I_{DC,ref}$ is optimized after the DC blocking, and the optimal value is 0.9995 p.u.. The curves of $\delta_{2,1}$ and $\delta_{5,1}$ with and without optimization are shown in Figure 8, and the analysis is given in Table 6. Compared with the objective function value without optimization, it is reduced by 1.66% with optimization. The optimization of $I_{DC,ref}$ improves the amplitude of the oscillations but has little effect on the convergence time.

5.3.2. Optimization to V_{ref} and $I_{DC,ref}$. In this case, V_{ref} and $I_{DC,ref}$ are optimized together after the DC blocking, and the optimal values are 0.9001 p.u. and 0.9342 p.u. respectively. As shown in Figure 9, the amplitude and the convergence time of the oscillations are improved, and the analysis is given in Table 7. λ_{apt} and λ_{cv} of $\delta_{2,1}$ are 7.78% and 13.64%, and those of $\delta_{5,1}$ are 8.86% and 9.40%. J is reduced from 40.44 to 39.30. The above results verify the suppression effect of the optimization to V_{ref} and $I_{DC,ref}$.

To verify the suppression effect of the SC on the angular oscillation, the analysis of the optimization to $I_{DC,ref}$ in Section 5.3.1 and that to V_{ref} with $I_{DC,ref}$ is compared in Figure 10. λ_{apt} and λ_{cv} of $\delta_{2,1}$ are increased by 6.25% and 13.64%, respectively, and those of $\delta_{5,1}$ are increased by 6.80% and 9.40%, respectively. Based on the above analysis, it is clear that the coordinated optimization to V_{ref} with $I_{DC,ref}$ further improves the oscillations.

5.3.3. Optimization to K_A, K_F, and T_F. With the set-points constant, the optimization to K_A, K_F, and T_F is implemented, and the optimal values are 211, 0.5002, and 0.4956 s respectively. As shown in Figure 11, the convergence time of $\delta_{5,1}$ is advanced from 38.51 s to 35.36 s and that of $\delta_{7,1}$ is advanced from 35.02 s to 31.84 s, and the amplitude is also improved. As given in Table 8, λ_{apt} and λ_{cv} of $\delta_{5,1}$ are 5.48% (0.32°) and 8.17% (3.15 s), respectively, and those of $\delta_{7,1}$ are 3.58% (0.22°) and 9.17% (3.18 s), respectively. J is reduced by 1.77% with the optimization.

Compared with the simulation results of optimization to V_{ref} and $I_{DC,ref}$ in Section 5.3.2, λ_{apt} and λ_{cv} of $\delta_{5,1}$ are reduced by 3.38% and 1.23%, respectively, and λ_J is reduced by 1.04%. The suppression effect of optimization to K_A, K_F, and T_F is weaker than that to V_{ref} and $I_{DC,ref}$.

5.3.4. Optimization to K_A, K_F, T_F, and V_{ref}. Control parameters and set-points of the SC are optimized together to suppress the oscillations, and the optimal values are 201, 0.5005, 0.0614 s, and 0.9004 p.u., respectively. The amplitude and the convergence time are improved in Figure 12, and

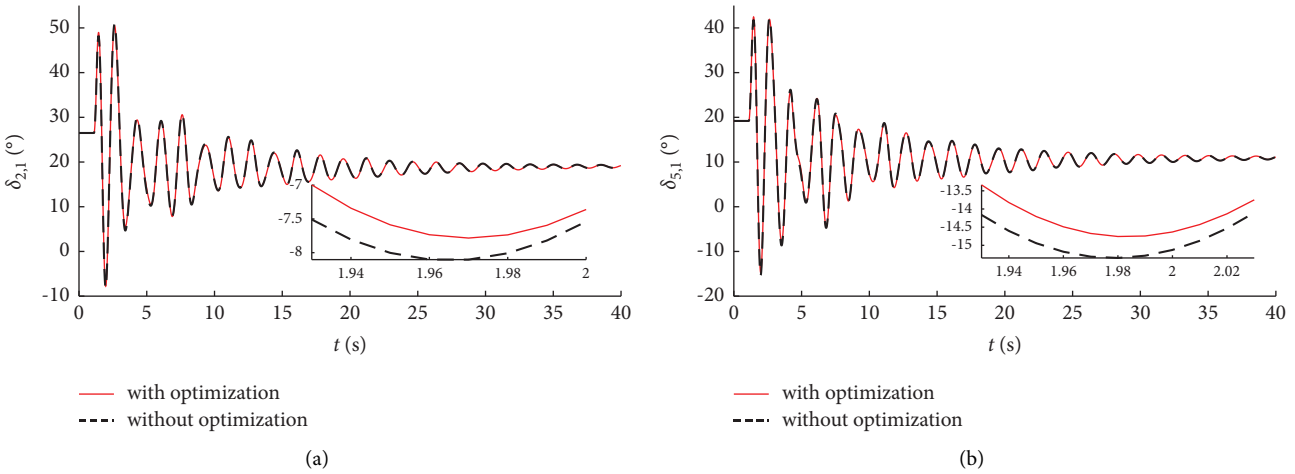

FIGURE 8: Power angle difference between SGs with and without optimization to $I_{DC,ref}$. (a) Power angle difference between #2 and #1 SGs. (b) Power angle difference between #5 and #1 SGs.

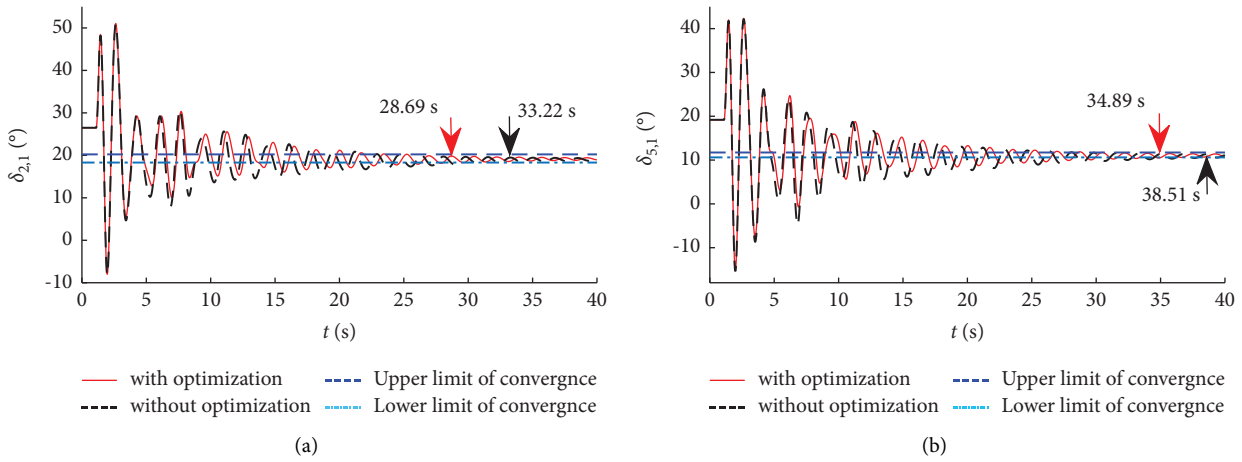

FIGURE 9: Power angle difference between SGs with and without optimization to V_{ref} and $I_{DC,ref}$. (a) Power angle difference between #2 and #1 SGs. (b) Power angle difference between #5 and #1 SGs.

TABLE 7: Effect analysis of optimization to V_{ref} and $I_{DC,ref}$.

	$\delta_{apt,woop}$ (°)	$\delta_{apt,wop}$ (°)	λ_{apt} (%)
$\delta_{2,1}$	5.24	4.83	7.78
$\delta_{5,1}$	5.90	5.38	8.86
	$t_{cv,woop}$ (s)	$t_{cv,wop}$ (s)	λ_{cv} (%)
$\delta_{2,1}$	33.22	28.69	13.64
$\delta_{5,1}$	38.51	34.89	9.40
	J_{woop}	J_{wop}	λ_J (%)
	40.44	39.30	2.81

Table 9 gives the analytic data of the simulation results. Λ_{apt} and λ_{cv} of $\delta_{5,1}$ are 17.46% (1.03°) and 15.53% (5.98 s), respectively, and those of $\delta_{7,1}$ are 18.48% (1.14°) and 11.94% (4.18 s), respectively. Compared with optimization to $I_{DC,ref}$ in Section 5.3.1, λ_{apt} and λ_{cv} of $\delta_{5,1}$ are increased by 15.4% and 15.53%, respectively, and λ_J is increased by 12.15%. It is found that the suppression effect of the optimization to K_A, K_F, T_F, and V_{ref} is better than that to $I_{DC,ref}$.

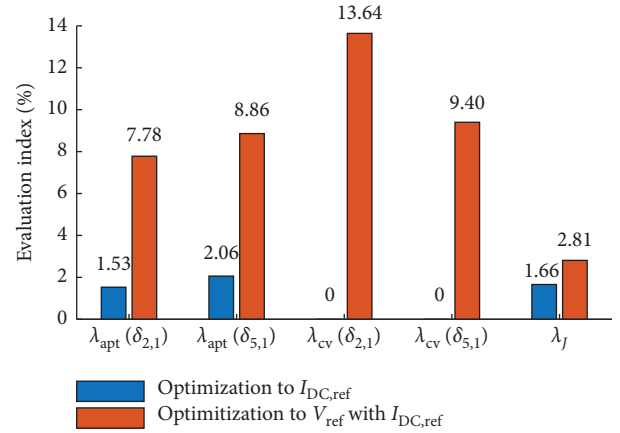

FIGURE 10: Comparison of optimization to $I_{DC,ref}$ and optimization to V_{ref} with $I_{DC,ref}$.

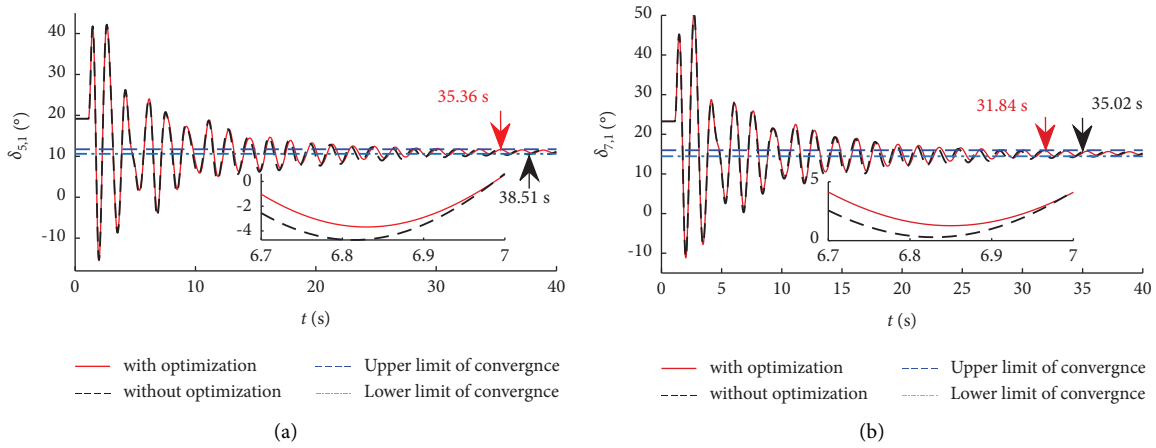

Figure 11: Power angle difference between SGs with and without optimization to K_A, K_F, and T_F. (a) Power angle difference between #5 and #1 SGs. (b) The power angle difference between #7 and #1 SGs.

Table 8: Effect analysis of optimization for K_A, K_F, and T_F.

	$\delta_{\text{apt,woop}}$ (°)	$\delta_{\text{apt,wop}}$ (°)	λ_{apt} (%)
$\delta_{5,1}$	5.90	5.58	5.48
$\delta_{7,1}$	6.17	5.95	3.58
	$t_{\text{cv,woop}}$ (s)	$t_{\text{cv,wop}}$ (s)	λ_{cv} (%)
$\delta_{5,1}$	38.51	35.36	8.17
$\delta_{7,1}$	35.02	31.84	9.17
	J_{woop}	J_{wop}	λ_J (%)
	40.44	39.72	1.77

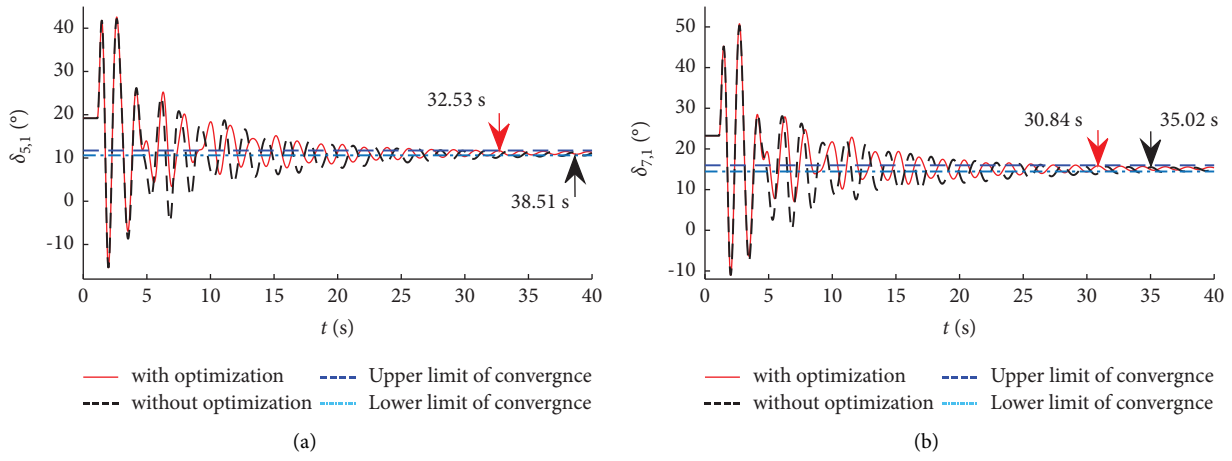

Figure 12: Power angle difference between SGs with and without optimization to K_A, K_F, T_F, and V_{ref}. (a) Power angle difference between #5 and #1 SGs. (b) The power angle difference between #7 and #1 SGs.

Table 9: Effect analysis of optimization for K_A, K_F, T_F, and V_{ref}.

	$\delta_{\text{apt,woop}}$ (°)	$\delta_{\text{apt,wop}}$ (°)	λ_{apt} (%)
$\delta_{5,1}$	5.90	4.87	17.46
$\delta_{7,1}$	6.17	5.03	18.48
	$t_{\text{cv,woop}}$ (s)	$t_{\text{cv,wop}}$ (s)	λ_{cv} (%)
$\delta_{5,1}$	38.51	32.53	15.53
$\delta_{7,1}$	35.02	30.84	11.94
	J_{woop}	J_{wop}	λ_J (%)
	40.44	34.85	13.81

Figure 13 shows the comparison of the simulation results in this section and those in Section 5.3.3. The effect of the coordinated optimization to K_A, K_F, T_F, and V_{ref} is better than that to K_A, K_F, and T_F. λ_{apt} and λ_{cv} of $\delta_{5,1}$ are increased by 11.98% and 7.36%, respectively, and those of $\delta_{7,1}$ are increased by 14.9% and 2.77%, respectively. And λ_J is increased by 12.04%.

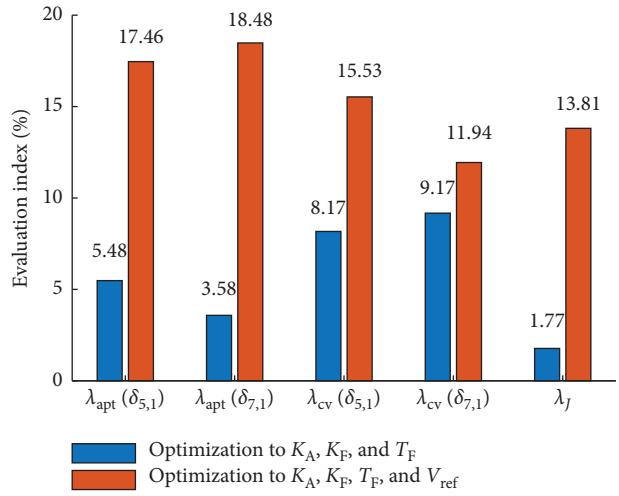

FIGURE 13: Comparison of optimization to K_A, K_F, and T_F and optimization to K_A, K_F, T_F, and V_{ref}.

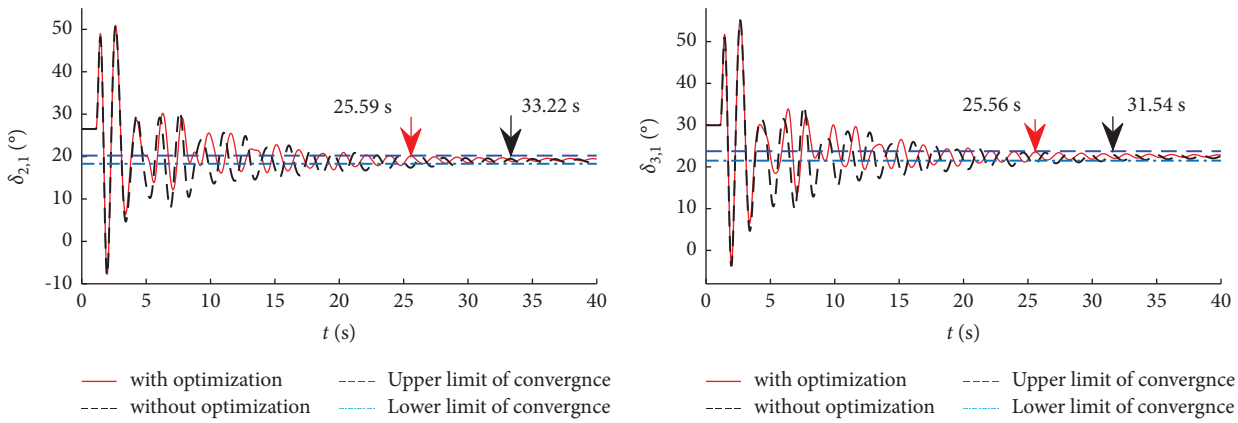

FIGURE 14: Power angle difference between SGs with and without coordinated optimization to K_A, K_F, T_F, V_{ref}, and $I_{DC,ref}$. (a) Power angle difference between #2 and #1 SGs. (b) Power angle difference between #3 and #1 SGs.

TABLE 10: Effect analysis of coordinated optimization to the CCC and the SC.

	$\delta_{apt,woop}$ (°)	$\delta_{apt,wop}$ (°)	λ_{apt} (%)
$\delta_{2,1}$	5.24	4.32	17.63
$\delta_{3,1}$	5.17	4.42	14.46
	$t_{cv,woop}$ (s)	$t_{cv,wop}$ (s)	λ_{cv} (%)
$\delta_{2,1}$	33.22	25.59	22.97
$\delta_{3,1}$	31.54	25.56	18.96
	J_{woop}	J_{wop}	λ_J (%)
	40.44	34.33	15.11

5.3.5. Optimization to K_A, K_F, T_F, V_{ref} and $I_{DC,ref}$. In this section, the proposed scheme is implemented. The optimal values of K_A, K_F, T_F, V_{ref}, and $I_{DC,ref}$ are 201, 0.5007, 0.0517 s, 0.9004 p.u. and 0.9998 p.u., respectively. As shown in Figure 14, the power angular oscillation is sharper without the optimization. To clearly describe the effect of the scheme, the analytic data of the simulation results are given in Table 10. λ_{apt} and λ_{cv} of $\delta_{2,1}$ are 17.63% (0.92°) and 22.97% (7.63 s), respectively, and those of $\delta_{3,1}$ are 14.46% (0.75°) and 18.96% (5.98 s), respectively. And λ_J is 15.11%, which is the largest one among the 5 groups of cases.

With the comparison of Tables 6–9, the effect of the coordinated optimization proposed in this paper is better than that of the optimization to control parameters or set-points. Compared with the simulation results in Section 5.3.2, λ_{apt} and λ_{cv} of $\delta_{2,1}$ are increased by 9.85% and 9.33%, respectively, and λ_J is increased by 12.3%. The above analysis validates the effectiveness of the proposed scheme for oscillation suppression.

5.3.6. Optimization to K_{pr} and K_{ir} of the CCC. As shown in Section 5.2, the mean trajectory sensitivities of K_{pr} and K_{ir} are smaller than other parameters. To illustrate the optimization effect of parameters with smaller sensitivities, the optimization to K_{pr} and K_{ir} is designed. The initial values of

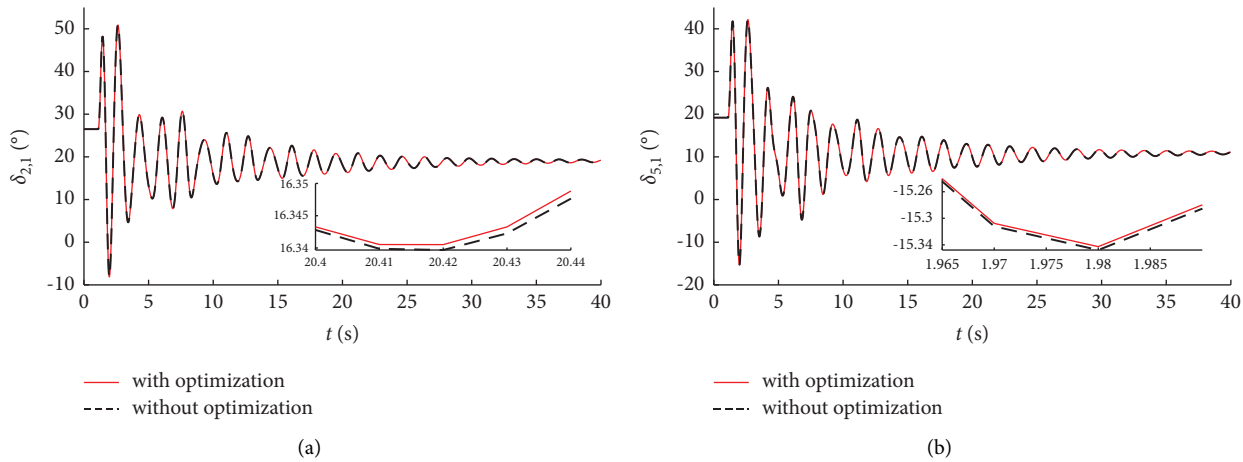

FIGURE 15: Power angle difference between SGs with and without optimization to K_{pr} and K_{ir} of the CCC. (a) Power-angle difference between #2 and #1 SGs. (b) Power-angle difference between #5 and #1 SGs.

TABLE 11: Effect analysis of coordinated optimization to K_{pr} and K_{ir} of the CCC.

	$\delta_{apt,woop}$ (°)	$\delta_{apt,wop}$ (°)	λ_{apt} (%)
$\delta_{2,1}$	5.24	5.20	0.76
$\delta_{5,1}$	5.90	5.85	0.84
	J_{woop}	J_{wop}	λ_J (%)
	40.44	40.12	0.79

TABLE 12: The optimization under scenarios with different faults.

Scenario	$a_{n,op}$				
	K_A	K_F	T_F (s)	V_{ref} (p.u.)	$I_{DC,ref}$ (p.u.)
1	201	0.5007	0.0517	0.9004	0.9998
2	200.3828	0.5010	0.05	0.9026	0.9999
3	200.9405	0.5053	0.0516	0.9151	0.9999
4	199.7838	0.5013	0.0555	0.9017	0.9999
a'	200.6124	0.5018	0.0518	0.9043	0.9998

TABLE 13: The comparison of the suppression effect of *a'* and $a_{\omega,op}$.

Scenario	λ_{ofv} (%)	
	$a_{n,op}$	a'
1	15.11	14.57
2	20.64	20.56
3	18.73	18.76
4	13.18	13.06

K_{pr} and K_{ir} are 1.0989 and 91.575, respectively, and the range are (0.9890, 1.2088) and (82.4175, 100.7325), respectively. The optimal values are 0.9902 and 82.4323. As shown in Figure 15 and Table 11, the optimization effect is slight, and there is almost no effect on the convergence time. And λ_J is 0.79%, which is smaller than the previous 5 groups of cases.

5.4. The Oscillations Suppression for Scenarios with Different Faults. In actual engineering, the fault scenarios are complex. Considering the research focus of this paper, the set of fault scenarios is simplified to four scenarios, i.e., Scenarios 1 to 4. φ_{IDN} of buses 9, 21, 26, and 28 are 3.7, 1.8, 4, and 2.4, respectively [43]. The severity indices of four scenarios calculated by (35) are 0.311, 0.151, 0.336, and 0.202, respectively. According to the sensitivity evaluation indices, the parameters to be optimized for the four scenarios are the same, i.e. K_A, K_F, T_F, V_{ref}, and $I_{DC,ref}$. The proposed scheme is implemented in Scenarios 2 to 4, and the optimization results for different scenarios (*an*, op and the weighting value *a'*) are shown in Table 12. As shown in Table 13, *a'* has a more acceptable effect for different scenarios when compared with $a_{n,op}$. Consequently, the applicability of the proposed scheme is verified with the severity indices of different faults.

6. Conclusion

To suppress the angular oscillations among SGs in the AC/HVDC power system, this paper proposes a coordinated optimization of the parameters and set-points of the constant current controller of the HVDC and the exciter of the SC based on the improved trajectory sensitivity. To differentiate periods of optimization, an improved analytical model of the trajectory sensitivity is proposed by introducing the step function to quantify the influence of the parameters on the angular oscillations. Based on the indication indices calculated by a mean trajectory sensitivity, the critical control parameters and the critical set-points of the constant current controller of the HVDC and the excitation system of the SC are newly decided to be optimized. With the objective of the minimal deviation of power angle differences, a coordinated multiparameter optimization model considering the periods of optimization is proposed and solved with the interior point method. Testing the proposed model in different scenarios reveals a suppression effect on the angular oscillations.

Some conclusions are found

(1) The accuracy of the improved TS is validated by comparing it with the perturbation method.

According to the numerical analysis, the maximum absolute error is only 5.22×10^{-5}, and the maximum relative error is only 1.82%.

(2) Based on the improved analytical expression of the TS, the proposed optimization scheme is suitable for control parameters and set-points with different periods of the optimization.

(3) Optimization to K_A, K_F, T_F, and V_{ref} can further improve the oscillations and shorten the convergence time, which has a better effect than optimization to K_A, K_F, and T_F.

(4) Optimization to V_{ref} with $I_{\text{DC,ref}}$ has a better effect on the oscillations than optimization to K_A, K_F, and T_F.

(5) By introducing the severity index of different scenarios and calculating the weighting value of the optimization results, the applicability of the proposed optimization model is verified.

(6) Compared with independent optimization, optimization to the HVDC and the SC has a better suppression effect.

(7) Compared with optimization to control parameters only, optimization of both control parameters and set-points has a better suppression effect. The adjustment range of set-points of the HVDC is reduced.

In the following study, oscillation suppression with parameter optimization at the sending and the receiving ends of the HVDC may be studied based on the proposed algorithm.

Nomenclature

Abbreviations

CCC: Constant current controller
cp: Control parameter
CEA: Constant extinction angle
cv: Convergence
DAE: Differential-algebraic equations
DFIG: Doubly-fed induction generators
Fau: Fault
HVDC: High-voltage direct-current
IDN: Importance degree of the node
pk, tr: Peak, trough
RV: Relative voltage
SC, SG: Synchronous condenser and generator
sp: Set-point
TS: Trajectory sensitivity

Notation

a: System parameters
U: Unit matrix
E: Electromotive force
e: Nonzero element
f_g: Differential and algebraic equations
G: Matrix of BFGS
H, N, M, L: Sub-Jacobian matrixes
k: Iteration number
NUM: Number
J: Objective function
P, Q: Active and reactive powers
p: One of system variables including state variables x and algebraic variables y
R, X: Resistance, reactance
S: Sensitivity
t: Time
V, I, θ: Voltage, current, angle
δ: Power angle
α: Control parameters or set-points
λ: Optimization ratio
φ_{IDN}: Index of the importance degree of the node
φ_{SEV}: Severity index of the scenario
ϕ_{ITM}: Intermediate variables for SC

Superscripts

min, max: Minimum and maximum values

Subscripts

A: Main regulator block
d, q: direct and quadrature axis
E: Exciter block
F: Feedback block
M: Measurement block
op: Optimization
s: Stator
x, y: x and y axis
woop: Without optimization
wop: With optimization
0: Initial value.

Data Availability

The data used to support the findings of this study are available from the author upon request.

Conflicts of Interest

The authors declare that they have no conflicts of interest.

Acknowledgments

This work was supported by the National Natural Science Foundation of China (NSFC) under Grant 51877061.

References

[1] R. Khezri, A. Oshnoei, A. Yazdani, and A. Mahmoudi, "Intelligent coordinators for automatic voltage regulator and power system stabiliser in a multi-machine power system," *IET Generation, Transmission & Distribution*, vol. 14, no. 23, pp. 5480–5490, 2020.

[2] S. Li, Z. Li, H. Zhang, Y. Shang, Y. Jiang, and Y. Song, "Control parameter optimization to DFIG-integrated power system based on extended trajectory sensitivity," *Acta Energiae Solaris Sinica*, vol. 42, no. 6, pp. 369–376, 2021.

[3] E. Munkhchuluun, L. Meegahapola, and A. Vahidnia, "Impact of active power recovery rate of DFIG wind farms on first swing rotor angle stability," *IET Generation, Transmission & Distribution*, vol. 14, no. 25, pp. 6041–6048, 2020.

[4] X. Sui, Y. Tang, H. He, and J. Wen, "Energy-storage-based low-frequency oscillation damping control using particle swarm optimization and heuristic dynamic programming," *IEEE Transactions on Power Systems*, vol. 29, no. 5, pp. 2539–2548, 2014.

[5] J. Bhukya and V. Mahajan, "Optimization of controllers parameters for damping local area oscillation to enhance the stability of an interconnected system with wind farm," *International Journal of Electrical Power & Energy Systems*, vol. 119, Article ID 105877, 2020.

[6] S. Latif, S. Irshad, M. Ahmadi Kamarposhti, H. Shokouhandeh, I. Colak, and K. Eguchi, "Intelligent design of multi-machine power system stabilizers (PSSs) using improved particle swarm optimization," *Electronics*, vol. 11, no. 6, p. 946, 2022.

[7] S. Li, Y. Li, D. Tao, Y. Liu, W. Yang, and Z. Wu, "Improved suppression measure to commutation failure at non-fault layer of UHVDC under hierarchical connection mode," *Power System Technology*, vol. 46, no. 11, pp. 4502–4514, 2022.

[8] L. Harnefors, N. Johansson, L. Zhang, and B. Berggren, "Interarea oscillation damping using active-power modulation of multiterminal HVDC transmissions," *IEEE Transactions on Power Systems*, vol. 29, no. 5, pp. 2529–2538, 2014.

[9] R. Eriksson, "A new control structure for multiterminal DC grids to damp interarea oscillations," *IEEE Transactions on Power Delivery*, vol. 31, no. 3, pp. 990–998, 2016.

[10] H. Liu, S. Zhang, L. Sun, C. Zhang, and X. Peng, "Transient stability analysis of the two-area with AC/DC paralleled interconnected power system in different operation," *Frontiers in Energy Research*, vol. 9, Article ID 755524, 2021.

[11] T. Wang, C. Li, D. Mi, Z. Wang, and Y. Xiang, "Coordinated modulation strategy considering multi-HVDC emergency for enhancing transient stability of hybrid AC/DC power systems," *CSEE Journal of Power and Energy Systems*, vol. 6, no. 4, pp. 806–815, 2020.

[12] Y. Zhang, M. Ding, P. Han, H. Sun, W. Yang, and Z. Chen, "Analysis of the interactive influence of the active power recovery rates of DFIG and UHVDC on the rotor angle stability of the sending-end system," *IEEE Access*, vol. 7, no. 1, pp. 79944–79958, 2019.

[13] N. Azizi, H. Moradi CheshmehBeigi, and K. Rouzbehi, "Optimal placement of direct current power system stabiliser (DCPSS) in multi terminal HVDC grids," *IET Generation, Transmission & Distribution*, vol. 14, no. 12, pp. 2315–2322, 2020.

[14] W. Wang, X. Xiong, M. Li, and R. Yu, "A flexible control strategy to prevent sending-end power system from transient instability under HVDC repetitive commutation failures," *IEEE Transactions on Power Systems*, vol. 35, no. 6, pp. 4445–4458, 2020.

[15] L. Yang, X. Xiao, and C. Pang, "Oscillation analysis of a DFIG-based wind farm interfaced with LCC-HVDC," *Science China Technological Sciences*, vol. 57, no. 12, pp. 2453–2465, 2014.

[16] S. Li, "Improvement to observability measures of LFO modes in power systems with DFIGs," *Frontiers in Energy*, vol. 15, no. 2, pp. 539–549, 2021.

[17] H. Yue, G. Shao, D. Xia, M. Sun, Y. Liu, and K. Wang, "Reactive power control strategy for UHVDC weak sending-end system considering overvoltage suppression," *Automation of Electric Power Systems*, vol. 44, no. 15, pp. 172–179, 2020.

[18] H. Li, S. Liu, H. Ji et al., "Damping control strategies of inter-area low frequency oscillation for DFIG-based wind farms integrated into a power system," *International Journal of Electrical Power & Energy Systems*, vol. 61, pp. 279–287, 2014.

[19] C. Wang, T. Jiang, F. Liu, H. Chen, and H. Lu, "Two-stage optimization control of transient overvoltage based on trajectory sensitivity," *Transactions of China Electrotechnical Society*, vol. 36, no. 9, pp. 1888–1913, 2021.

[20] O. Kotb, M. Ghandhari, R. Eriksson, R. Leelaruji, and V. K. Sood, "Stability enhancement of an interconnected AC/DC power system through VSC-MTDC operating point adjustment," *Electric Power Systems Research*, vol. 151, pp. 308–318, 2017.

[21] A. Mehrizi-Sani and R. Iravani, "Online set point modulation to enhance microgrid dynamic response: theoretical foundation," *IEEE Transactions on Power Systems*, vol. 27, no. 4, pp. 2167–2174, 2012.

[22] H. Ghaffarzadeh, C. Stone, and A. Mehrizi-sani, "Predictive set point modulation to mitigate transients in lightly damped balanced and unbalanced systems," *IEEE Transactions on Power Systems*, vol. 32, no. 2, pp. 1041–1049, 2016.

[23] S. Li and H. Zhang, "Improved eigen-sensitivity with respect to transfer function of DFIG-PSS in wind power systems," *Electric Power Components and Systems*, vol. 48, no. 16, pp. 1735–1746, 2021.

[24] J. Ma, S. Wang, Y. Li, and Y. Qiu, "Power system multi-parameter small signal stability analysis based on 2nd order perturbation theory," *International Journal of Electrical Power & Energy Systems*, vol. 67, pp. 409–416, 2015.

[25] R. Azizipanah-Abarghooee, M. Malekpour, Y. Feng, and V. Terzija, "Modeling DFIG-based system frequency response for frequency trajectory sensitivity analysis," *International Transactions on Electrical Energy Systems*, vol. 29, no. 4, p. e2774, 2019.

[26] H. Fayazi, M. Moazzami, B. Fani, and G. Shahgholian, "A first swing stability improvement approach in microgrids with synchronous distributed generators," *International Transactions on Electrical Energy Systems*, vol. 31, no. 4, Article ID e12816, 2021.

[27] S. Yuan and D. Fang, "Robust PSS parameters design using a trajectory sensitivity approach," *IEEE Transactions on Power Systems*, vol. 24, no. 2, pp. 1011–1018, 2009.

[28] Y. Tang, P. Ju, H. He, C. Qin, and F. Wu, "Optimized control of DFIG-based wind generation using sensitivity analysis and particle swarm optimization," *IEEE Transactions on Smart Grid*, vol. 4, no. 1, pp. 509–520, 2013.

[29] R. Nagi, X. Huan, and Y. C. Chen, "Bayesian inference of parameters in power system dynamic models using trajectory sensitivities," *IEEE Transactions on Power Systems*, vol. 37, no. 2, pp. 1253–1263, 2022.

[30] C. Mishra, "Critical clearing time sensitivity for differential-algebraic power system model," *IEEE Transactions on Power Systems*, vol. 36, no. 4, pp. 3153–3162, 2021.

[31] S. Li, X. Yu, Y. Hua, W. Han, and C. Song, "Suppression to power system in weakly damped modes based on sensitivity to reactive output of DFIG," *High Voltage Engineering*, vol. 48, no. 4, pp. 1356–1364, 2022.

[32] M. Yazdanian, A. Mehrizi-Sani, R. R. Seebacher, K. Krischan, and A. Muetze, "Smooth reference modulation to improve

dynamic response in electric drive systems," *IEEE Transactions on Power Electronics*, vol. 33, no. 7, pp. 6434–6443, 2018.

[33] Y. Luo, J. Yao, T. Zhang, J. Pei, and F. Zhang, "Coordinated control strategy of large-scale wind power generation sending system under mono-polar block fault," *Transactions of China Electrotechnical Society*, vol. 34, no. 19, pp. 4108–4118, 2019.

[34] S. Hashemi, H. Lesani, and M. R. Aghamohammadi, "An integrated approach for incorporation of voltage and transient stabilities into optimal power flow study," *Electric Power Systems Research*, vol. 206, Article ID 107784, 2022.

[35] X. Luo, F. Li, L. Fan et al., "Influence of synchronous condensers on operation characteristics of Double-infeed LCC-HVDCs," *Processes*, vol. 9, no. 10, p. 1704, 2021.

[36] X. Wang, Q. Chen, and Y. Zhang, "Modal analysis on system stability of UHVDC hierarchical connection to AC grid," *Power System Technology*, vol. 42, no. 9, pp. 2869–2878, 2018.

[37] S. Li, N. Zhang, and H. Zhang, "AC/UHVDC system reliability and sensitivity evaluation considering state transition of wind power and power adjustment of UHVDC," *Power System Technology*, vol. 45, no. 6, pp. 2342–2351, 2021.

[38] I. Adebayo, A. A. Jimoh, and A. Yusuff, "Voltage stability assessment and identification of important nodes in power transmission network through network response structural characteristics," *IET Generation, Transmission & Distribution*, vol. 11, no. 6, pp. 1398–1408, 2017.

[39] S. Li, T. Fang, H. Zhang, W. Han, C. Song, and A. Zhang, "Damping to electromechanical oscillation modes in DFIG-integrated system based on sensitivity of electromechanical loop participation ratio," *High Voltage Engineering*, vol. 47, no. 14, pp. 3414–3425, 2021.

[40] S. Li, H. Zhao, H. Zhou, and A. Zhang, "Reliability sensitivity-based optimization for a UHVDC transmission system with preventive maintenance," *Power System Protection and Control*, vol. 50, no. 3, pp. 68–75, 2022.

[41] Y. Fang, "Reflections on stability technology for reducing risk of system collapse due to cascading outages," *Journal of Modern Power Systems and Clean Energy*, vol. 2, no. 3, pp. 264–271, 2014.

[42] X. Dong, J. Luo, X. Cui, H. Li, H. Xia, and X. Li, "Whole control time and its constitution of security and stability control system," *Automation of Electric Power Systems*, vol. 42, no. 5, pp. 163–168, 2018.

[43] D. Zhu, R. Wang, W. Cheng, J. Duan, and H. Wang, "Critical transmission node identification method based on improved PageRank algorithm," *Power System Protection and Control*, vol. 50, no. 5, pp. 86–93, 2022.